Journal of Engineering Mathematics **45:** 135–154, 2003.

Periodic orbit analysis of two dynamical systems for electrical engineering applications

M. KARIMI-GHARTEMANI[1] and A. K. ZIARANI[1,†]
[1]*Department of Electrical and Computer Engineering, University of Toronto, Toronto, Ontario, Canada; e-mail: masoud@ele.utoronto.ca*
[2]*Department of Electrical and Computer Engineering, Clarkson University, Potsdam, New York, U.S.A.; e-mail: aziarani@clarkson.edu*

Received 11 September 2001; accepted in revised form 30 July 2002

Abstract. Mathematical properties of two nonlinear adaptive filters for electrical engineering applications are presented. These filters are designed to extract a desired sinusoidal component of a given periodic signal and estimate its amplitude, phase angle and frequency. Two sets of non-autonomous ordinary differential equations govern the dynamics of the filters. It is shown that each of the filters possesses a unique and stable periodic orbit. The averaging theorem is used to prove the uniqueness and stability of the periodic orbit of one of the filters. Uniqueness and stability of the periodic orbit of the other filter are proven using the Poincaré map theorem. Computer simulations and numerical results are presented to provide numerical verification of the theoretical proofs, and finally experimental results of the laboratory implementation of the filters are presented.

Key words: averaging method, periodic/almost periodic solutions, Poincaré mapping, signal analysis

1. Introduction

Signal analysis plays an important role in deriving crucial characteristics of the processes in a large class of engineering problems. Conventional methods such as Fourier analysis have been widely employed in various engineering disciplines for transforming time-domain signals into the frequency domain. The importance of frequency-domain representation of signals lies in the ability to determine the energy content of the individual signal components in the frequency domain. Required information for the analysis, design, control and protection of a variety of engineering systems can be obtained based on the extraction of individual components of signals in the frequency domain [1–5].

A nonlinear adaptive filter capable of on-line signal analysis for electrical-engineering-systems protection, control and quality enhancement was recently introduced in [6]. The filter is capable of focusing on a specific frequency component of its input signal and extracting it. The mechanism of the filter is such that it extracts the amplitude and phase of the sinusoidal component of its input signal for which its internal operating point is preset. The mathematical model describing the dynamics of the filter assumes variations in both the amplitude and phase of the preset component; therefore, we shall refer to it as the Amplitude Phase Model (APM). The structure of the filter is adaptive in the sense that it tracks variations of the input signal. In other words, if the amplitude or phase of the input signal undergoes variations with time, the output of the filter follows those variations without requiring any change to be made in

[†]author for correspondence

its internal structure. The filter has a wide range of applications in electrical engineering in general and in power systems in particular [6].

As an extension to the filter described by APM, another nonlinear adaptive filter assuming variations of amplitude, phase and frequency is proposed in [7], which we shall refer to as Amplitude Phase Frequency Model (APFM).

Two sets of non-autonomous differential equations govern the dynamics of the filters. It will be shown that each of the filters possesses a unique and stable periodic orbit. The sketch of the proofs of these properties for the APM filter was presented in a condensed form in [8] for an audience with little interest in the detailed mathematical proofs. In this paper, the complete mathematical aspects of the proofs are presented. The emphasis is on the theoretical and mathematical aspects rather than their implementation and applications.

In this paper, two theorems are proven to substantiate the mathematical properties of the filters. The averaging theorem is used to prove the uniqueness and stability of a periodic orbit for APM. Uniqueness and stability of the periodic orbit for the APFM are proven using the Poincaré-map theorem.

The structure of the paper is as follows. At first, a brief introduction to the subject of signal analysis in electrical engineering is provided for the reader unfamiliar with engineering applications. Section 3 outlines the steps of derivation of the governing differential equations of APM and APFM. The theorems summarizing the properties of the filters together with details of their proofs are presented in Sections 4 and 5 for the APM and APFM filters, respectively. Computer simulations and numerical results are presented in Section 6 to provide numerical verification of the theoretical proofs. Laboratory implementation of APM together with some experimental results are presented in Section 7 to provide an introduction to the engineering application of the mathematical discussions presented in this paper. Finally, some open problems concerning the filters which may be of interest to mathematics community are proposed in Section 8. A brief review of the important theorems used in the proofs throughout the paper is provided in the appendix for a quick and easy reference.

2. Signal analysis in electrical engineering: an overview

Signals in electrical engineering jargon are basically functions of time, and are usually voltages/currents at the input/output of (or within) electrical systems. Ideally, power generators supply sinusoidal signals at a fixed frequency of 50 Hz or 60 Hz (called the *fundamental* frequency) which under various conditions may be distorted. Traditionally, Fourier-series analysis has been used to extract the frequency spectrum (the set of all frequency components) of the signals. The Fourier-series representation of a signal is the summation of single sine functions at the frequencies of integer multiples of the fundamental frequency. The first term in the summation is the fundamental component and the rest are the distortion added to the pure sinusoidal signal. Each single term in the summation with a frequency of n ($n > 1$) times the fundamental frequency is called the n^{th} *harmonic*. The coefficient of each single sine term is usually called the *amplitude* and its angle is called the *phase* of that component. Sometimes, the time-independent part of the phase is considered as the phase of the signal. The amplitude of each harmonic component gives a measure of the energy content of the signal at the corresponding frequency. The quality of a signal is judged on the basis of the amplitudes and/or orders of the harmonics present in the signal. The pure sine function has no

harmonic content. The more *distorted* (*i.e.*, deviated from the pure sine function) a signal is, the more harmonic content it has.

A filter in electrical engineering terminology is a projection from a set of signals to another set of signals with a more limited frequency spectrum. For example, an *ideal notch filter* is a filter whose range is only a single sine function; in other words, it extracts a fixed preset harmonic component of its input signal. This particular example is of extreme importance in disturbance detection and quality enhancement applications where the quality of the signals is measured on the basis of the extracted harmonic contents. The study of the quality of the signals in the frequency domain is feasible once the individual components of the signals are extracted by the use of notch filters.

Different methods have been employed to construct notch filters. Traditionally, analog circuitry have been used. With the advancement in the digital computing technology, discrete methods such as Discrete Fourier Transform (DFT) have been used for digital implementation. The main drawback of these methods is their fixed-frequency design limitation in the sense that the notch frequency is designed to be fixed once and forever. There is yet another problem with the application of such filters. An ideal notch filter is the one which is sensitive exclusively to its center frequency. A filter thus designed will be inoperative when a slight change in the fundamental frequency of the signal occurs which is a usual phenomenon in electrical systems. Therefore, the better the filter is designed, the more inoperative it becomes if any change in the fundamental frequency occurs.

The most promising and idealistic concept is a filter with a sharp notch but with the capability of adaptive tracking of the frequency even when the frequency of the signal undergoes a slight change or if any disturbance in the electrical properties of the system occurs. The fact that signals may undergo variations with time makes the issue of the ideal filter complicated. For example, in a power system the fundamental frequency is not time-independent and may have small variations, in the range of fractions of Hertz. Moreover, transient signals that may be of very short duration (such as spikes caused by lightning) or relatively long duration (such as capacitor switching oscillations) may be superimposed to the signals from time to time. These phenomena lead one to consider the electrical signals as *almost periodic* signals rather than perfectly *periodic*. Another aspect that should be considered in the design of such filters is the practical aspect of the problem. A suitable method is the one that can be implemented in real-time without requiring complex algorithms and tools. Robustness of the system is highly enhanced when the algorithm remains simple.

One approach to construct such an ideal filter is to introduce an adaptive mechanism into a linear notch filter in order to adjust the filter center frequency [9]. Our method aims at extracting the fundamental sinusoidal component of a distorted signal based on the direct estimation of the amplitude and the phase (frequency) of the signal. Once the fundamental component is extracted, all the superimposed components (*i.e.* distortion) are also available. Performance of this design has been demonstrated and its superior performance is observed [6, 8].

3. Derivation of governing differential equations

Let $u(t)$ represent a voltage or current signal. This function is usually continuous and almost periodic. A sinusoidal component of this function, $y(t) = A\sin(\omega t + \delta)$, is of interest where A is the amplitude, ω is the frequency (in rad/s), δ is the constant phase and $\phi(t) = \omega t +$

δ represents the total phase of this component. Ideally, parameters A, ω, and δ are fixed quantities; but, in practice, this assumption does not hold true.

In a typical situation in power engineering, $u(t)$ has a general form of

$$u(t) = u_o(t) + \sum_{i \neq 1} A_i \sin(i\omega_o t + \delta_i), \tag{1}$$

in which the terms within the summation are harmonic components. In practice, all the parameters in (1) may undergo variations with time. In other words, a *nonstationary* or equivalently, a *time-varying* case is encountered.

Let $\mathcal{M}$ be a continuous manifold containing all sinusoidal signals defined as

$$\mathcal{M} = \left\{ y(t,\theta),\, t \in \mathbb{R},\ \theta_i \in [\theta^i_{\min},\ \theta^i_{\max}],\ i = 1, \cdots, n,\ y : \text{Sinusoid} \right\},$$

where $\theta(t) = [\theta_1(t), \cdots, \theta_n(t)]^T$ is the vector of parameters which belongs to the parameter space

$$\Theta = \{[\theta_1, \cdots, \theta_n]^T \mid \theta_i \in [\theta^i_{\min}, \theta^i_{\max}],\ i = 1, \cdots, n\}$$

and the superscript T denotes matrix transposition.

Our aim is to find an element in $\mathcal{M}$ which is the closest to the desired sinusoidal component of signal $u(t)$. The solution has to be an orthogonal projection of $u(t)$ onto manifold $\mathcal{M}$, or equivalently it has to be an optimum θ which minimizes a distance function d between $y(t, \theta(t))$ and $u(t)$, *i.e.*,

$$\theta_{\text{opt}} = \arg \min_{\theta(t) \in \Theta} d[y(t, \theta(t)), u(t)].$$

Without being concerned about the mathematical correctness of the definition of the least squares error, which strictly speaking has to map onto the set of real numbers rather than functions, we use the instantaneous distance function d [10]:

$$d^2(t, \theta(t)) = [u(t) - y(t, \theta(t))]^2 = e^2(t).$$

Hence, the cost function is defined as $J(\theta(t), t) = d^2(t, \theta(t))$. Although the cost function is not necessarily quadratic, the parameter vector θ is estimated using the gradient descent method,

$$\frac{\mathrm{d}\theta(t)}{\mathrm{d}t} = -\mu \frac{\partial [J(t, \theta(t))]}{\partial \theta(t)}, \tag{2}$$

where the positive diagonal matrix μ is the algorithm regulating constant matrix. The values of the entries of this matrix control the convergence rate as well as the stability of the algorithm. Given a quadratic cost function, it is clear that the algorithm employing this method converges to the minimum solution for the cost function. In more complex cases than those involving quadratic functions, the gradient descent method may still achieve minimization although this is not true in general. The choice of the gradient descent method for the minimization process is intuitive and no rigorous justification can be presented at this point; its application is a reflection of an intuitive predisposition towards its common use. Global convergence of the gradient descent method is guaranteed for quadratic distance functions; otherwise, its convergence has to be directly proven.

4. Amplitude Phase Model (APM)

In APM, the aim is to extract the amplitude and phase of the fundamental sinusoidal component of the input signal. Its salient feature is that it follows time-variations of both the amplitude and the phase of the input signal.

APM assumes that the fundamental frequency of the input signal is a fixed quantity. However, this model also has the capability of tracking small variations in the fundamental frequency of the input signal as well. In most practical situations, variations in the fundamental frequency of the input signal are small and therefore can be adequately followed by APM. A more advanced model, aiming at accommodating larger variations in the fundamental frequency of the input signal, is presented in Section 5.

4.1. Mathematical model

With respect to the assumption of constant frequency, the parameter vector is chosen to be $\theta = [\hat{A}, \hat{\phi}]$, *i.e.*, the amplitude and phase angle of the desired component. The desired fundamental component is $u_o(t) = A \sin \phi(t)$ where A denotes the amplitude and $\phi = \omega_o t + \delta$ represents the phase of this component. Its fundamental frequency is $f_o = 1/T_o = \omega_o/2\pi$ which is normally 50 or 60 Hz.

Following the derivation steps of Section 3, the dynamics of the proposed filter is found to described by the following two differential and one algebraic equations:

$$\dot{\hat{A}}(t) = -2\mu_1 \hat{A}(t) \sin^2(\hat{\phi}(t)) + 2\mu_1 \sin(\hat{\phi}(t))\, u(t), \tag{3}$$

$$\dot{\hat{\phi}}(t) = -\mu_2 \hat{A}^2(t) \sin(2\hat{\phi}(t)) + 2\mu_2 \hat{A}(t) \cos(\hat{\phi}(t))\, u(t) + \omega_o, \tag{4}$$

$$y(t) = \hat{A}(t) \sin(\hat{\phi}(t)), \tag{5}$$

where the caret on top denotes an estimated value and the dot on top represents the derivative with respect to time. The estimated phase is $\hat{\phi}(t) = \omega_o t + \hat{\delta}(t)$. The parameters μ_1 and μ_2 are positive constants called step sizes and determine the speed of the filter.

In engineering terminology, the function $u(t)$ which represents voltage or current is considered as the input signal and the function $y(t)$ generated by this system is the output signal of the filter. The two differential equations together represent a dynamical system in which $u(t)$ is an external force.

It will be shown that, for a proper choice of the parameters μ_1 and μ_2, the dynamical system represented by the above two differential equations possesses a unique asymptotically stable periodic orbit which lies in a neighborhood of the orbit associated with the fundamental component of the function $u(t)$. In terms of the engineering performance of the system, this indicates that the output of the system $y(t)$ will approach the fundamental component of the input signal $u(t)$; in other words, the system is a filter which extracts the fundamental component of its input signal.

Moreover, the slow variations of parameters in $u(t)$ are tolerated by the system, *i.e.*, the filter is adaptive and the output follows variations in the input.

4.2. PERIODIC ORBIT ANALYSIS OF APM

Equations (3) and (4) are framed in polar coordinates and are represented in this section by the more familiar variables ρ and ϕ. The input $u(t)$ is also replaced by an external force $f(t)$ which is a more familiar concept in dynamical systems theory. Rewriting the two differential equations of the system using the new notations, we have

$$\frac{\mathrm{d}\rho}{\mathrm{d}t} = -2\mu_1\rho\sin^2\phi + 2\mu_1\sin\phi\ f(t), \tag{6}$$

$$\frac{\mathrm{d}\phi}{\mathrm{d}t} = -\mu_2\rho^2\sin(2\phi) + 2\mu_2\rho\cos\phi\ f(t) + \omega_o. \tag{7}$$

The phase plane diagram of this dynamical system is considered in polar coordinate system in which a pure sinusoidal function $f_o(t) = \rho_o\sin(\omega_o t + \delta_o)$ is represented by a circle centered at the origin and having a radius ρ_o. When the general form (1) for the external force $f(t)$ is assumed, this dynamical system is supposed to extract its fundamental component $f_o(t)$.

The periodic-orbit analysis of this dynamical system is carried out in Theorem 1. We will prove that the solution of (6) and (7) approaches the desired values A_o and ϕ_o regardless of the initial conditions. Thus, the output function $y(t)$ asymptotically approaches the input function $f(t)$. In terms of polar coordinates of (ρ, ϕ), it is shown that APM has a unique stable periodic orbit a neighborhood of $f_o(t)$ which coincides with $f_o(t)$ when no higher order harmonics are present.

The step-sizes μ_1 and μ_2 determine the time speed of the convergence to the solution of the differential equations. If the parameters in the input function vary with time, the desired solution will follow those variations provided that the speed of the convergence to the solutions, determined by the step sizes, is high enough.

Theorem 1. Let $f(t) = A_o\sin(\omega_o t + \delta_o) + g(t)$ where A_o, ω_o, and δ_o are real constants and $g(t)$ is an arbitrary T_o–periodic bounded continuous function which has no frequency component at ω_o. For an appropriate choice of parameters μ_1 and μ_2, the APM dynamics described by Equations (6) and (7) has a unique periodic orbit $\gamma(t)$ in (ρ, ϕ) plane in a neighborhood of $f_o(t) = A_o\sin(\omega_o t + \delta_o)$. This neighborhood is determined by the function $g(t)$ and the parameters μ_1 and μ_2 in APM. Moreover, this periodic orbit is asymptotically stable. The periodic orbit coincides with $f_o(t)$ when $g(t)$ is zero.

Proof. Define $\mu_1 = \epsilon\hat{\mu}_1$ and $\mu_2 = \epsilon\hat{\mu}_2$ where $\epsilon \ll 1$ is a positive real number. When the new notations are used, the dynamics (6) and (7) becomes

$$\frac{\mathrm{d}\rho}{\mathrm{d}t} = \epsilon\{-2\hat{\mu}_1\rho\sin^2(\omega_o t + \delta) + 2\hat{\mu}_1\sin(\omega_o t + \delta)\,[f_o(t) + g(t)]\}, \tag{8}$$

$$\frac{\mathrm{d}\delta}{\mathrm{d}t} = \epsilon\{-\hat{\mu}_2\rho^2\sin(2(\omega_o t + \delta)) + 2\hat{\mu}_2\rho\cos(\omega_o t + \delta)\,[f_o(t) + g(t)]\}, \tag{9}$$

where δ is defined as $\delta = \phi - \omega_o t$. Equations (8) and (9) are in the standard form of the *averaging theorem*, namely

$$\dot{X} = \epsilon F(X, t, \epsilon) \tag{10}$$

where $F : \mathbb{R}^2 \times \mathbb{R} \times \mathbb{R}^+ \longrightarrow \mathbb{R}^2$ is of class C^r, $r \geq 2$, bounded on bounded sets, and of period $T_o > 0$ in t if we define

$$\begin{aligned} X &= \begin{pmatrix} \rho \\ \delta \end{pmatrix}, \\ F(X, t, \epsilon) &= \begin{pmatrix} -2\hat{\mu}_1 \rho \sin^2(\omega_o t + \delta) + 2\hat{\mu}_1 \sin(\omega_o t + \delta)\,[f_o(t) + g(t)] \\ -\hat{\mu}_2 \rho^2 \sin(2(\omega_o t + \delta)) + 2\hat{\mu}_2 \rho \cos(\omega_o t + \delta)[f_o(t) + g(t)] \end{pmatrix}. \end{aligned} \tag{11}$$

The well-known averaging theorem in general form is reviewed in Appendix A.

The associated averaged system is defined as

$$\dot{X}_a = \epsilon \frac{1}{T_o} \int_0^{T_o} F(X_a, t, 0)\, \mathrm{d}t := \epsilon \bar{F}(X_a), \tag{12}$$

where the new variable X_a is the 'averaged' value of X. Thus,

$$\begin{aligned} \dot{\rho}_a = \; & \epsilon \frac{1}{T_o} \int_0^{T_o} \{-2\hat{\mu}_1 \rho_a \sin^2(\omega_o t + \delta_a) + 2\hat{\mu}_1 A_o \sin(\omega_o t + \delta_a) \sin(\omega_o t + \delta_o)\} \mathrm{d}t \\ & + 2\hat{\mu}_1 \sin(\omega_o t + \delta_a) g(t)\} \mathrm{d}t = -\mu_1 \rho_a + \mu_1 A_o \cos(\delta_a - \delta_o), \end{aligned}$$

$$\begin{aligned} \dot{\delta}_a = \; & \epsilon \frac{1}{T_o} \int_0^{T_o} \{-\hat{\mu}_2 \rho_a^2 \sin(2(\omega_o t + \delta_a)) + 2\hat{\mu}_2 A_o \rho_a \cos(\omega_o t + \delta_a) \sin(\omega_o t + \delta_o)\} \mathrm{d}t \\ & + 2\hat{\mu}_2 \rho_a \cos(\omega_o t + \delta_a) g(t)\} \mathrm{d}t = -\mu_2 A_o \rho_a \sin(\delta_a - \delta_o). \end{aligned}$$

Note that $g(t)$ is T_o-periodic and has no frequency component at ω_o; therefore, based on Fourier series expansion, it can be written as

$$g(t) = \sum_{n \neq 1} g_n \sin(n\omega_o t + \delta_n). \tag{13}$$

Thus, simple calculations show that

$$\int_0^{T_o} \sin(\omega_o t + \delta_a) g(t) \mathrm{d}t = \int_0^{T_o} \sin(\omega_o t + \delta_a) g(t) \mathrm{d}t = 0.$$

The averaged system has the following dynamics:

$$\begin{cases} \dot{\rho}_a &= -\mu_1 \rho_a + \mu_1 A_o \cos(\delta_a - \delta_o) \\ \dot{\delta}_a &= -\mu_2 A_o \rho_a \sin(\delta_a - \delta_o) \end{cases}, \tag{14}$$

which yields

$$\bar{F}(\rho_a, \delta_a) = \begin{pmatrix} -\hat{\mu}_1 \rho_a + \hat{\mu}_1 A_o \cos(\delta_a - \delta_o) \\ -\hat{\mu}_2 A_o \rho_a \sin(\delta_a - \delta_o) \end{pmatrix}. \tag{15}$$

The averaged system clearly has a fixed point at $P_o = (A_o, \delta_o)$. The linearized system about $P_o = (A_o, \delta_o)$ is

$$(\epsilon \bar{F})|_{P_o} = \begin{pmatrix} -\mu_1 & 0 \\ 0 & -\mu_2 A_o^2 \end{pmatrix}. \tag{16}$$

The derivative matrix is non-singular which implies that the fixed point P_o is locally unique. The eigenvalues of the matrix are $-\mu_1$ and $-\mu_2 A_o^2$ and both are negative. Therefore, this fixed point is asymptotically stable. With reference to the averaging theorem, it is concluded that the system has a unique asymptotically stable periodic orbit $\gamma_\epsilon(t)$ which lies in an $\epsilon-$ neighborhood of $\gamma_o(t)$, the desired component of $f(t)$. For $g = 0$, it is easy to verify that $f_o(t)$ is a solution for the differential equations of APM.

The solution of the linearized system (denoted by $X_{a_\ell}(t)$) initiated at $X_{a_\ell}(t_o)$ is

$$\begin{pmatrix} \rho_{a_\ell}(t) \\ \delta_{a_\ell}(t) \end{pmatrix} = \begin{pmatrix} \rho_{a_\ell}(t_o)\ \exp[-\mu_1(t-t_o)] \\ \delta_{a_\ell}(t_o)\ \exp[-\mu_2 A_o^2(t-t_o)] \end{pmatrix}. \tag{17}$$

The eigenvalues of the system, *i.e.*, $(-\mu_1, -\mu_2 A_o^2)$, determine the speed of the system in approaching the solution. The larger the values of μ_1 and μ_2 are chosen, the faster the amplitude and phase of the output convergence to those of the desired component.

So far, no assumption has been made on the form of $g(t)$ except its periodicity which is sufficient (and not necessary!) for the application of the averaging theorem. This distortion element can be in the form of harmonics or any other periodic oscillation. However, as it is shown by the simulations in Section 6, many other possible sorts of distortions such as spikes and oscillating transients and signal fluctuations which are not periodic may be applied without causing any malfunctioning in the operation of the filter.

5. Amplitude Phase Frequency Model (APFM)

In APM, the frequency ω_o is assumed to be a fixed quantity. Therefore, the performance of the filter represented by APM when the frequency also happens to be changing with time can not be rigorously predicted. Simulations in Section 6 show the insensitivity of APM to slight variations in frequency. Therefore, APM is adequate for most practical situations. A more advanced dynamics to accommodate larger variations of the frequency is presented in this section.

5.1. Mathematical model

In APFM, the vector of parameters is defined as $\theta = [\hat{A}, \hat{\omega}, \hat{\phi}]$, *i.e.*, the amplitude, frequency and phase angle of the desired component. Following the same derivation strategy presented in Section 3 and with some modifications to conclude a time-invariant system, the dynamical system of APFM is obtained and expressed by the following third-order system:

$$\dot{\hat{A}} = -2\mu_1 \hat{A} \sin^2 \hat{\phi} + 2\mu_1 \sin \hat{\phi}\ f(t), \tag{18}$$

$$\dot{\hat{\omega}} = -\mu_2 \hat{A}^2 \sin(2\hat{\phi}) + 2\mu_2 \hat{A} \cos \hat{\phi}\ f(t), \tag{19}$$

$$\dot{\hat{\phi}} = \hat{\omega} + \mu_3 \dot{\hat{\omega}}. \tag{20}$$

The system is transformed into the spherical-coordinate system by replacing $(\hat{A}, \hat{\omega}, \hat{\phi})$ by (ρ, θ, ϕ) and we obtain

$$\frac{\mathrm{d}\rho}{\mathrm{d}t} = -2\mu_1 \rho \sin^2 \phi + 2\mu_1 \sin \phi\ f(t), \tag{21}$$

$$\frac{\mathrm{d}\theta}{\mathrm{d}t} = -\mu_2\rho^2\sin(2\phi) + 2\mu_2\rho\cos\phi\ f(t), \tag{22}$$

$$\frac{\mathrm{d}\phi}{\mathrm{d}t} = \theta + \mu_3\frac{\mathrm{d}\theta}{\mathrm{d}t}. \tag{23}$$

5.2. Periodic orbit analysis of APFM

Let $f(t) = f_o(t) + g(t)$ where $f_o(t) = A_o\sin\phi_o(t)$ and $\phi_o(t) = \omega_o t + \delta_o$. Rewrite (21), (21) and (23) as

$$\frac{\mathrm{d}\rho}{\mathrm{d}t} = -2\mu_1\rho\sin^2\phi + 2\mu_1 A_o\sin(\omega_o t + \delta_o)\sin\phi + 2\mu_1\sin\phi g(t), \tag{24}$$

$$\frac{\mathrm{d}\theta}{\mathrm{d}t} = -\mu_2\rho^2\sin(2\phi) + 2\mu_2 A_o\sin(\omega_o t + \delta_o)\rho\cos\phi + 2\mu_2\rho g(t), \tag{25}$$

$$\frac{\mathrm{d}\phi}{\mathrm{d}t} = \theta + \mu_3\frac{\mathrm{d}\theta}{\mathrm{d}t}. \tag{26}$$

The following theorem deals with the existence, uniqueness and stability of a periodic orbit for this dynamical system. The proofs are based on the Poincaré theorem. According to the Poincaré theorem, the behavior of the dynamical system near its periodic orbit can be investigated using a discrete map. The fixed points of this map correspond to the periodic orbits of the main dynamics and their stability types are equivalent.

Theorem 2. Let $f(t) = A_o\sin(\omega_o t + \delta_o) + g(t)$ where A_o, ω_o, and δ_o are real constants and $g(t)$ is an arbitrary T_o–periodic bounded continuous function which has no frequency component at ω_o. For a proper choice of parameters $\{\mu_i, i = 1, 2, 3\}$, the APFM dynamics described by Equations (24) to (26) has a unique periodic orbit $\gamma(t)$ in (ρ, θ, ϕ) space in a neighborhood of $f_o(t) = A_o\sin(\omega_o t + \delta_o)$. This neighborhood is determined by the function $g(t)$ and the parameters μ_1 to μ_3 in APFM. Moreover, this periodic orbit is asymptotically stable. The periodic orbit coincides with $f_o(t)$ when $g(t)$ is zero.

Proof. The main ideas are based on the Poincaré map theorem, a review of which is provided in Appendix B. Since APFM is a time-periodic system, we need to rewrite its equations in the form of an autonomous equation in four dimensions by defining the function

$$\begin{aligned} &\gamma_1 : \mathbb{R}^1 \longrightarrow S^1, \\ &\qquad t \longmapsto \omega_o t, \ \bmod 2\pi, \end{aligned} \tag{27}$$

where S^1 denotes the circle. Replacing t with γ_1/ω_o in (24) to (26) and including $\mathrm{d}\gamma_1/\mathrm{d}t = \omega_o$ result in a four-dimensional autonomous system.

A suitable *cross-section* to obtain the Poincaré map is

$$\Sigma_\epsilon = \{(\rho, \theta, \phi, \gamma) \ : \ \mid \rho - A_o \mid < \epsilon, \ \mid \theta - \omega_o \mid < \epsilon^3, \ \mid \phi - \delta_o \mid < \epsilon, \ \gamma = \delta_o\}. \tag{28}$$

The suitability of this section is clarified during the proof.

Consider the initial point $(\rho_1, \theta_1, \phi_1, \delta_o) \in \Sigma_\epsilon$. After the period time $T_o = 2\pi/\omega_o$, this point will be transformed to $(\rho_2, \theta_2, \phi_2, \delta_o + 2\pi)$ under the flow of the dynamics. We will show that this second point is also in Σ_ϵ. The Poincaré map is defined as follows:

$$\begin{aligned} P:\ & \Sigma_\epsilon \longrightarrow \Sigma_\epsilon \\ & (\rho_1, \theta_1, \phi_1) \longmapsto (\rho_2, \theta_2, \phi_2). \end{aligned} \tag{29}$$

Suppose μ_1 and μ_2 are *small* and define $\mu_1 = \epsilon\hat{\mu}_1$ and $\mu_2 = \epsilon^2\hat{\mu}_2$. With this definition, all the terms in (24) have a coefficient of ϵ and all the terms in (25) have a coefficient of ϵ^2 on the trajectory connecting $(\rho_1, \theta_1, \phi_1)$ to $(\rho_2, \theta_2, \phi_2)$. The values of $\dot{\theta}$ and $\dot{\rho}$ can be written as $\mathcal{O}(\epsilon^2)$ and $\mathcal{O}(\epsilon)$. Therefore,

$$\rho(t) = \rho_1 + \int_0^t \dot{\rho}(\tau)\mathrm{d}\tau = \rho_1 + \mathcal{O}(\epsilon) \quad \forall t \in I = [0, T_o], \tag{30}$$

$$\theta(t) = \theta_1 + \int_0^t \dot{\theta}(\tau)\mathrm{d}\tau = \theta_1 + \mathcal{O}(\epsilon^2) \quad \forall t \in I = [0, T_o]. \tag{31}$$

Also, note that $\forall t \in I = [0, T_o]$

$$\phi(t) = \phi_1 + \int_0^t \dot{\phi}(\tau)\mathrm{d}\tau = \delta_o + \int_0^t [\theta(\tau) + \mu_3\dot{\theta}(\tau)]\mathrm{d}\tau = \phi_1 + \theta_1 t + \mathcal{O}(\epsilon^2). \tag{32}$$

Now, we compute the Poincaré map using the following integration formulas

$$\rho_2 = \rho_1 + \int_0^{T_o} \dot{\rho}(t)\mathrm{d}t, \theta_2 = \theta_1 + \int_0^{T_o} \dot{\theta}(t)\mathrm{d}t, \phi_2 = \phi_1 + \int_0^{T_o} \dot{\phi}(t)\mathrm{d}t.$$

Substituting from (30), (31) and (32), we obtain

$$\begin{aligned} \rho_2 &= \rho_1 - 2\mu_1 \int_0^{T_o} [\rho_1 + \mathcal{O}(\epsilon)] \sin^2[\theta_1 t + \phi_1 + \mathcal{O}(\epsilon^2)]\mathrm{d}t \\ &\quad + 2\mu_1 A_o \textstyle\int_0^{T_o} \sin(\omega_o t + \delta_o) \sin[\theta_1 t + \phi_1 + \mathcal{O}(\epsilon^2)]\mathrm{d}t \\ &\quad + 2\mu_1 \textstyle\int_0^{T_o} \sin[\theta_1 t + \phi_1 + \mathcal{O}(\epsilon^2)] g(t)\mathrm{d}t \\ &= \rho_1 - 2\mu_1\rho_1[\frac{T_o}{2} - \frac{\sin(T_o\theta_1)\cos(T_o\theta_1 + 2\phi_1)}{2\theta_1}] \\ &\quad + 2\mu_1 A_o \frac{\sin(T_o\theta_1/2)\cos(T_o\theta_1/2 + \phi_1 - \delta_o)}{\theta_1 - \omega_o} \\ &\quad - 2\mu_1 A_o \frac{\sin(T_o\theta_1/2)\cos(T_o\theta_1/2 + \phi_1 + \delta_o)}{\theta_1 + \omega_o} + \mathcal{O}(\epsilon^2) \\ &= \rho_1 - \mu_1 T_o \rho_1 + \mu_1 T_o A_o + \mathcal{O}(\epsilon^2) \end{aligned} \tag{33}$$

and

$$\begin{aligned} \theta_2 &= \theta_1 - \mu_2 \textstyle\int_0^{T_o} [\rho_1 + \mathcal{O}(\epsilon)]^2 \sin[2\theta_1 t + 2\phi_1 + \mathcal{O}(\epsilon^2)]\mathrm{d}t \\ &\quad + 2\mu_2 A_o \textstyle\int_0^{T_o} [\rho_1 + \mathcal{O}(\epsilon)] \sin(\omega_o t + \delta_o) \cos[\theta_1 t + \phi_1 + \mathcal{O}(\epsilon^2)]\mathrm{d}t \\ &\quad + 2\mu_2 \textstyle\int_0^{T_o} [\rho_1 + \mathcal{O}(\epsilon)] \cos[\theta_1 t + \phi_1 + \mathcal{O}(\epsilon^2)] g(t)\mathrm{d}t \\ &= \theta_1 - \mu_2\rho_1^2 \frac{\sin(T_o\theta_1/2)\sin(T_o\theta_1/2 + 2\phi_1)}{\theta_1} \\ &\quad + 2\mu_2 A_o \rho_1 \frac{\sin(T_o\theta_1/2 + \phi_1 + \delta_o)\sin(T_o\theta_1/2)}{\omega_o + \theta_1} \\ &\quad + 2\mu_2 A_o \rho_1 \frac{\sin(T_o\theta_1/2 + \phi_1 - \delta_o)\sin(T_o\theta_1/2)}{\omega_o - \theta_1} + \mathcal{O}(\epsilon^3). \end{aligned} \tag{34}$$

Note that in calculating the above integrals we have made use of the following two facts: (1) $g(t)$ is a T_o-periodic function with no frequency component at ω_o and it can be represented as (1), and (2) both $(\rho_o, \theta_o, \phi_0)$ and $(\rho_1, \theta_1, \phi_1)$ are on the section Σ_ϵ specified in (28). Thus, simple calculations result in the following identities:

$$\int_0^{T_o} \sin[\theta_1 t + \phi_1 + \mathcal{O}(\epsilon^2)] g(t) \mathrm{d}t = \mathcal{O}(\epsilon^3),$$

$$\int_0^{T_o} \cos[\theta_1 t + \phi_1 + \mathcal{O}(\epsilon^2)] g(t) \mathrm{d}t = \mathcal{O}(\epsilon^3),$$

$$\frac{\sin(\frac{\pi\theta_1}{\omega_o})}{\theta_1 - \omega_o} = -\frac{\pi}{\omega_o} + \mathcal{O}(\epsilon^6).$$

Calculation of ϕ_2 is the last step in obtaining the Poincaré map:

$$\phi_2 = \phi_1 + \int_0^{T_o} [\theta + \mu_3 \dot{\theta}] \mathrm{d}t = \phi_1 + \int_0^{T_o} \theta(t) \mathrm{d}t + \mu_3(\theta_2 - \theta_1).$$

We need to obtain $\theta(t)$ and then integrate it over the period I.

$$\begin{aligned}
\theta_2(t) &= \theta_1 - \mu_2 \textstyle\int_0^t [\rho_1 + \mathcal{O}(\epsilon)]^2 \sin[2\theta_1\tau + 2\phi_1 + \mathcal{O}(\epsilon^2)] \mathrm{d}\tau \\
&\quad + 2\mu_2 A_o \textstyle\int_0^t [\rho_1 + \mathcal{O}(\epsilon)] \sin(\omega_o \tau + \delta_o) \cos[\theta_1\tau + \phi_1 + \mathcal{O}(\epsilon^2)] \mathrm{d}\tau \\
&\quad + 2\mu_2 \textstyle\int_0^t [\rho_1 + \mathcal{O}(\epsilon)] \cos[\theta_1\tau + \phi_1 + \mathcal{O}(\epsilon^2)] g(\tau) \mathrm{d}\tau \\
&= \theta_1 - \mu_2 \rho_1^2 \frac{\cos(2\phi_1) - \cos(2\theta_1 t + 2\phi_1)}{2\theta_1} \\
&\quad + \mu_2 A_o \rho_1 \frac{\cos(\phi_1 + \delta_o) - \cos[(\omega_o + \theta_1)t + \phi_1 + \delta_o]}{\omega_o + \theta_1} \\
&\quad + 2\mu_2 A_o \rho_1 \frac{\cos(\phi_1 - \delta_o) - \cos[(\omega_o - \theta_1)t - \phi_1 + \delta_o]}{\omega_o - \theta_1} + \mathcal{O}(\epsilon^3).
\end{aligned}$$

The integral of $\theta_2(t)$ is:

$$\begin{aligned}
&\int_0^{T_o} \theta_2(t) dt = \theta_1 T_o - \frac{\mu_2 T_o \rho_1^2}{2\theta_1} \cos(2\phi_1) + \frac{\mu_2 T_o A_o \rho_1}{\omega_o + \theta_1} \cos(\phi_1 + \delta_o) \\
&+ 2\mu_2 A_o \rho_1 \frac{T_o(\omega_o - \theta_1)\cos(\phi_1 - \delta_o) - \sin(\phi_1 - \delta_o) - \sin[(\omega_o - \theta_1)T_o - \phi_1 + \delta_o]}{(\omega_o - \theta_1)^2} \\
&+ \mathcal{O}(\epsilon^3)
\end{aligned}$$

Substituting this in (35) results in

$$\begin{aligned}
\phi_2 \;=\; & \phi_1 + \theta_1 T_o - \frac{\mu_2 T_o \rho_1^2}{2\theta_1}\cos(2\phi_1) + \frac{\mu_2 T_o A_o \rho_1}{\omega_o + \theta_1}\cos(\phi_1 + \delta_o) \\
& + 2\mu_2 A_o \rho_1 \frac{T_o(\omega_o - \theta_1)\cos(\phi_1 - \delta_o) - \sin(\phi_1 - \delta_o) - \sin[(\omega_o - \theta_1)T_o - \phi_1 + \delta_o]}{(\omega_o - \theta_1)^2} \\
& - \mu_2 \mu_3 \rho_1^2 \frac{\sin(T_o\theta_1/2)\sin(T_o\theta_1/2 + 2\phi_1)}{\theta_1} \\
& + 2\mu_2 \mu_3 A_o \rho_1 \frac{\sin(T_o\theta_1/2 + \phi_1 + \delta_o)\sin(T_o\theta_1/2)}{\omega_o + \theta_1} \\
& + 2\mu_2 \mu_3 A_o \rho_1 \frac{\sin(T_o\theta_1/2 + \phi_1 - \delta_o)\sin(T_o\theta_1/2)}{\omega_o - \theta_1} + \mathcal{O}(\epsilon^3).
\end{aligned} \tag{36}$$

The Poincaré map is specified by (33), (34) and (35). Note that $\theta_1 T_o = 2\pi + \mathcal{O}(\epsilon^3)$, mod $2\pi = \mathcal{O}(\epsilon^3)$.

Consider the Poincaré map as $P = Id + F$ where Id is the identity function. At point $(\rho, \theta, \phi, \epsilon) = (A_o, \omega_o, \delta_o, 0)$, function F vanishes; *i.e.*, $F(A_o, \omega_o, \delta_o, 0) = 0$ and its derivative map is in the form of

$$\begin{pmatrix} X_1 & 0 \\ X_2 & X_3 \end{pmatrix},$$

where X_i's are equal to

$$X_1 = -\mu_1 T_o,$$

$$X_2 = \begin{pmatrix} 0 \\ -\dfrac{1}{4\pi}\mu_2 T_o^2 A_o \cos(2\delta_o) \end{pmatrix},$$

$$X_3 = \begin{pmatrix} -\dfrac{1}{2}\mu_2 A_o^2 T_o^2 & -\dfrac{1}{2}\mu_2 A_o^2 T_o^2 \\ -\dfrac{1}{48\pi^2}\mu_2 T_o^3 A_o^2[16\pi^2 - 3\cos(2\delta_o)] & -\mu_2 T_o^2 A_o^2(1 - \dfrac{\sin(2\delta_o)}{4\pi}) - \mu_2\mu_3 T_o A_o^2 \end{pmatrix}.$$

One of the eigenvalues, associated with X_1, is equal to $\lambda_1 = -\mu_1 T_o$. Let the other two, corresponding to X_3, be λ_2 and λ_3. Then,

$$\lambda_1 + \lambda_2 = -\frac{1}{2}\mu_2 A_o^2 T_o^2 - \mu_2 T_o^2 A_o^2(1 - \frac{\sin(2\delta_o)}{4\pi}) - \mu_2\mu_3 T_o A_o^2$$

$$\begin{aligned}
\lambda_1\lambda_2 \;=\; & -\frac{1}{2}\mu_2 A_o^2 T_o^2 \{-\mu_2 T_o^2 A_o^2(1 - \frac{\sin(2\delta_o)}{4\pi}) \\
& -\mu_2\mu_3 T_o A_o^2 + \frac{1}{48\pi^2}\mu_2 T_o^3 A_o^2[16\pi^2 - 3\cos(2\delta_o)]\} \\
=\; & \frac{1}{2}\mu_2^2 T_o^3 A_o^4 \{\mu_3 - \Omega(T_o, \delta_o)\}
\end{aligned}$$

where

$$\Omega(T_o, \delta_o) = -T_o[1 - \frac{\sin(2\delta_o)}{4\pi}] + \frac{T_o^2}{48\pi^2}[16\pi^2 - 3\cos(2\delta_o)].$$

Obviously, $\lambda_1 + \lambda_2 < 0$. It is easy to obtain a condition on μ_3 to make $\lambda_1\lambda_2 > 0$ for all δ_o, *i.e.*,

$$\mu_3 > \max(\max_{\delta_o \in (0,2\pi]} \Omega(T_o, \delta_o), 0).$$

A simple calculation leads to

$$\max_{\delta_o \in (0,2\pi]} \Omega(T_o, \delta_o) = \frac{T_o^2}{48\pi^2}[16\pi^2 + \frac{3T_o}{\sqrt{16\pi^2 + T_o^2}}] + T_o(\frac{4\pi}{\sqrt{16\pi^2 + T_o^2}} - 1).$$

For small values of T_o, this expression can be well approximated by $T_o^2/3$, *i.e.*, around 0·00015 for power system frequency. With this proper choice of μ_3, the derivative matrix is non-singular with all three eigenvalues having negative real parts; therefore, the derivative map is one-to-one. It can be concluded, from the implicit function theorem (Appendix C), that equation $F(\rho_1, \theta_1, \phi_1, \epsilon) = 0$ has a unique solution $(\rho_1(\epsilon), \theta_1(\epsilon), \phi_1(\epsilon))$ in an ϵ–neighborhood of $(A_o, \omega_o, \delta_o)$ for which

$$(\rho_1(0), \theta_1(0), \phi_1(0)) = (A_o, \omega_o, \delta_o).$$

Note that this solution of equation $F(\rho_1, \theta_1, \phi_1, \epsilon) = 0$ corresponds to the fixed point of Poincaré map and hence to the periodic orbit of the original dynamics in (24), (25) and (26).

To study the stability of the periodic orbit of the system, consider the linearized set of Poincaré equations about $\gamma_o(t)$:

$$DP\,|_{\gamma_o(t)} = \begin{pmatrix} 1 & 0 & 0 \\ 0 & 1 & 0 \\ 0 & 0 & 1 \end{pmatrix} + DF\,|_{(A_o,\omega_o,\delta_o,0)}\ . \tag{37}$$

The eigenvalues of the linearized Poincaré map which determine the stability type of this periodic orbit are computed as

$$\begin{cases} 1 + \lambda_1 = 1 - \mu_1 T_o + \mathcal{O}(\epsilon^2) \\ 1 + \lambda_2 = 1 + \lambda_2(\mu_2, \mu_3) + \mathcal{O}(\epsilon^3) \\ 1 + \lambda_3 = 1 + \lambda_3(\mu_2, \mu_3) + \mathcal{O}(\epsilon^3) \end{cases}\ . \tag{38}$$

Note that both of the above eigenvalues lie within the unit circle provided that μ_1 and μ_2 are small positive numbers and μ_3 satisfies the given condition. Parameter μ_1 has a direct effect on the value of λ_1 and the magnitudes of the other two is controlled by μ_2. Therefore, the obtained unique periodic orbit is asymptotically stable.

Our computer simulations show that a μ_1 as large as $2/T_o$, *i.e.*, around 100 for power system frequency, maintains the stability. This is in conformity with (38). Large values of μ_2 can also maintain the stability provided that μ_3 is not too small. Perfect conformity of the theoretical results with the numerical results obtained by the computer simulations is observed. All this means that we imposed the ambiguous condition of being *small enough* on the parameters to proceed with the proof. Practical extent of the range of parameters can be obtained by means of numerical examinations for every particular application.

6. Computer simulations

A number of computer simulations are performed using MATLAB^{TM} simulation software to provide numerical verification of the proofs. These simulations are meant to show the behavior

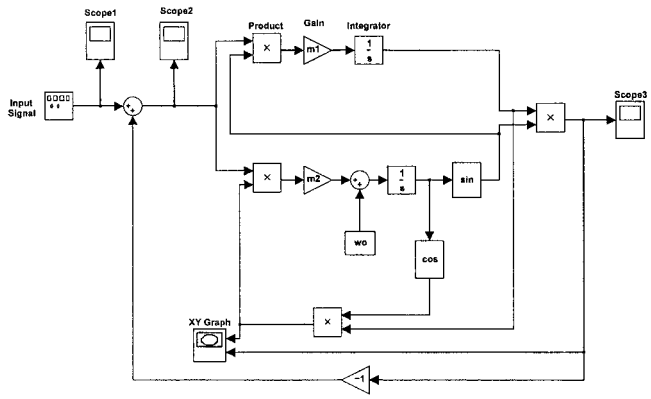

Figure 1. Block diagram representation of the digital implementation of the APM dynamics.

of the mathematically analyzed dynamical systems. In both cases of APM and APFM, the performance of the filters is studied by applying different input signals to the filters. In each case, the simulation shows the convergence of the output to the desired component of the input signal (normally, the fundamental component) as is expected from the mathematical analysis.

Figure 1 shows the block diagram of the simulated digital implementation of APM. The diagram is easy to follow to verify its equivalency to the dynamical system described by the differential equations in Section 4.

At first, we apply a purely sinusoidal signal to the input of the APM filter. The output (according to Theorem 1) is expected to follow the input. Figure 2 shows the performance of the filter. It is clear that the output approaches the input. The speed of this approach is controlled by the values of the step sizes μ_1 and μ_2.

A typical signal with high harmonic content is a square wave. In a numerical experiment, the input to APM filter is taken to be a square wave. Figure 3 shows convergence of the output to the fundamental component of the input signal.

The main advantage of the these filters over conventional methods is their ability to adaptively track variations of the input signal. In Figure 4, the amplitude of the input signal is suddenly changed. It is observed that the output adapts itself to these variations with a speed controlled by μ_1 and μ_2 and follows the input.

As another example of the adaptive tracking feature of APM, the frequency of the input signal is slightly changed (refer to Figure 5). Although the mathematical modeling of the APM filter is not meant to accommodate such variations in the frequency, it is clearly observed that it has the capability to adaptively track even variations in the frequency.

Numerical experiments similar to those of the APM filter were carried out to show the performance of the APFM filter. In all cases, similar results were obtained. In order to demonstrate the existence of the periodic orbit of this dynamics, one example of the performance of the filter is shown in Figure 6. A planar perspective of the phase portrait is considered in this graph.

Another simulation showing the frequency tracking feature of APFM is presented in Figure 7. The input signal to the system is a pure sinusoid at frequency of 100 Hz and then suddenly changes to a distorted sinusoid with frequency of 400 Hz. The three-dimensional phase portrait of the system, shown in Figure 7, confirms the tracking properties of APFM.

According to Theorem 2, the system tends to instability for smaller values of μ_3. This effect is verified by a simulation in Figure 8. Frequency of the signal undergoes a step change

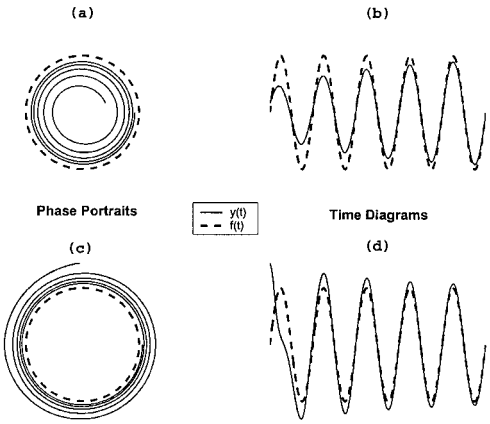

Figure 2. This figure shows the performance of the filter modeled by APM for a pure sinusoidal signal at the input. The speed at which the output approaches the desired component of the input is controlled by the values of μ_1 and μ_2. Two cases of amplitude initial conditions less than the desired value (parts a and b) and greater than the desired value (parts c and d) are considered.

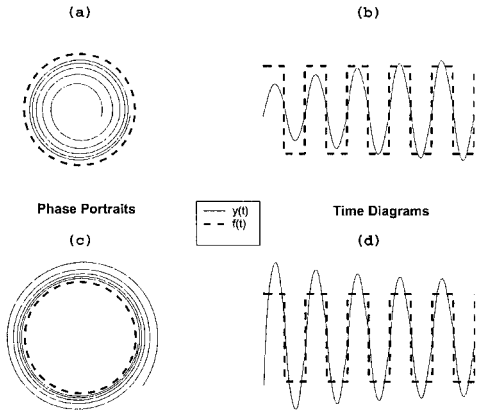

Figure 3. This figure shows the performance of the filter modeled by APM for a square wave at the input. The filter extracts the fundamental component of the input signal. Two cases of amplitude initial conditions less than the desired value (parts a and b) and greater than the desired value (parts c and d) are considered.

from 50 to 60 Hz and APFM is used to estimate the frequency. Four values of μ_3 are tested: $\mu_3 = 0{\cdot}032, 0{\cdot}016, 0{\cdot}008$ and $0{\cdot}004$. It is clearly observed that smaller values of μ_3 create more oscillatory responses.

.

7. Laboratory implementation

This section presents the performance of the proposed filter configurations based on a digital realization of them. The digital set-up includes (a) a signal generator to generate different input signals and (b) a Universal High-Performance (UHP40) controller platform [14]. The heart of the UHP40 is a floating point Digital Signal Processor (DSP). The program that represents the filter function is written in C programming language and is downloaded into the DSP board. The input signal is digitized using an analog to digital converter and is applied to the DSP. The output signal is the fundamental component of the input signal extracted by the adaptive nonlinear filter.

Figure 9 shows the input and the output of the filter when a square wave is applied to the input and the filter is adjusted to extract the fundamental component of its input signal.

8. Some open problems

There are a few mathematically unsolved problems concerning the dynamical systems presented in this paper. These problems exist similarly for both APM and APFM systems. This section presents some of such problems which may be of interest to the reader.

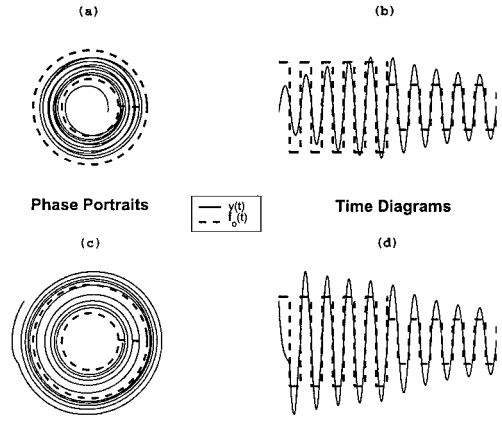

Figure 4. This figure demonstrates the adaptive feature of the APM filter. The amplitude of the input signal suddenly changes, and the filter adapts itself quickly and follows the input. Two cases of amplitude initial conditions less than the desired value (parts a and b) and greater than the desired value (parts c and d) are considered.

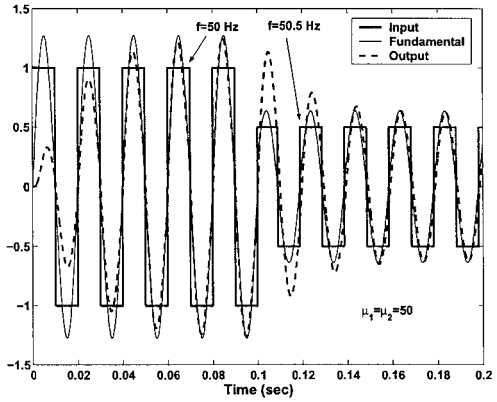

Figure 5. Somewhat unexpected adaptive feature of the APM filter is demonstrated in this figure. Slight variations in frequency are tracked by the filter.

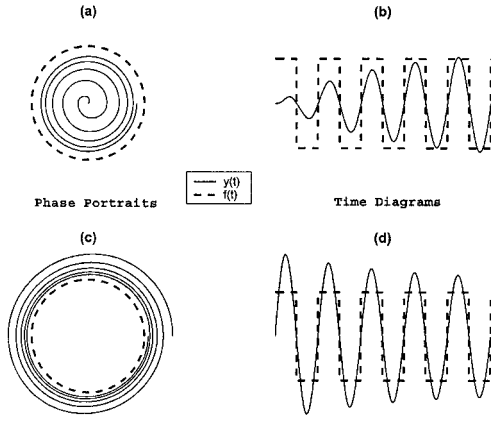

Figure 6. This figure shows the performance of the filter modeled by APFM for a square wave at the input. The filter extracts the fundamental component of the input signal. Two cases of amplitude initial conditions less than the desired value (parts a and b) and greater than the desired value (parts c and d) are considered.

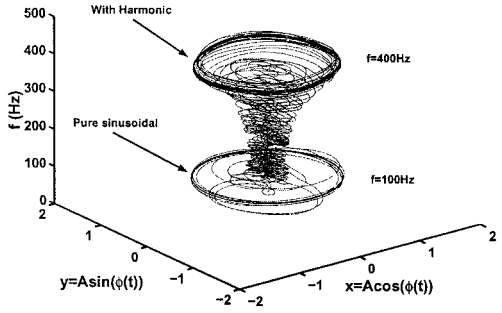

Figure 7. This figure shows the performance of the filter modeled by APFM during a frequency jump. The input to the system is a pure sinusoid at the frequency of 100 Hz and then suddenly changes to a distorted sinusoid with frequency of 400 Hz.

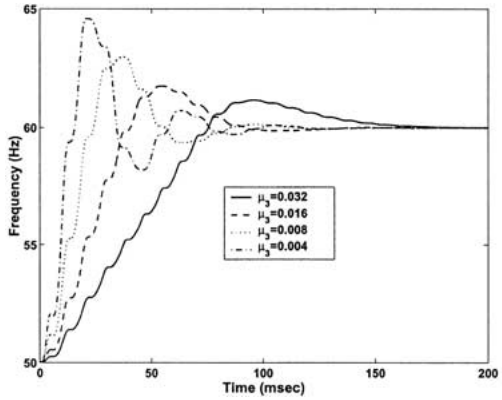

Figure 8. This figure verifies the effect of μ_3 on the performance of the APFM when is used as a frequency estimator. As expected by the Theorem 2, reducing μ_3 moves the system towards instability.

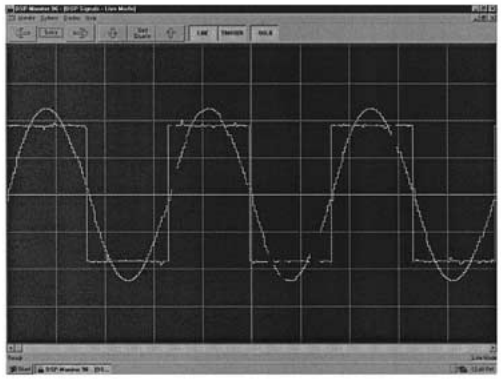

Figure 9. Performance of the digital implementation of the APM filter when the input is a square wave and the filter is adjusted to extract the fundamental component of its input is demonstrated in this figure.

1. Only the local proof of the theorems is presented in this paper. In practice we have observed that within a range of values of the amplitude and phase angle (and frequency), the convergence is achieved. Therefore, global proof of the theorems – under specified conditions – is of interest.
2. The theorems cover only the T_o-periodic signals. However, it is of interest to have similar theorems (or a general theorem) covering more general cases. An example is the case where the input signal is comprised of one fundamental component at frequency ω_o and another frequency component at $\alpha\omega_o$ with a non-integer α. Our computer simulations show that different scenarios occur depending on the value of α. Few examples are presented below for the case of APM system.
   $\alpha = 2{\cdot}5$: This case creates an orbit with a double period. Figure 10 shows this orbit together with the ideal orbit (circle).
   $\alpha = 1{\cdot}6$: This case creates an orbit the period of which is five times the original one. Figure 11 shows this orbit together with the ideal orbit (circle).
   $\alpha = \sqrt{3}$: The flow associated with this value seems to be rotating forever, without closing itself. Figure 12 shows this flow.

Similar phenomena are observed in the case of APFM. Figure 13 shows a double-period orbit case and another orbit the period of which is eight times the period of the original one for the case of APFM. In all the graphs in this section, the frequency is 400 Hz and the signal $g(t)$ is deliberately chosen large to provide good visualization of the orbits.

The general conclusion is that for an arbitrary α, it seems that there is either a periodic orbit (with period NT_o, where N is a function of α) or an open-orbit. In both cases, they are located on a torus. Periodic orbit seems to happen for rational α. The open-orbit happens for irrational α.

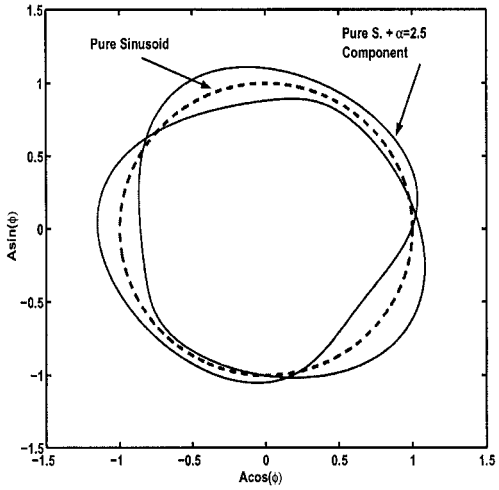

Figure 10. The periodic orbit of APM associated with the input $u(t) = u_o(t) + \sin(2{\cdot}5\omega_o t)$

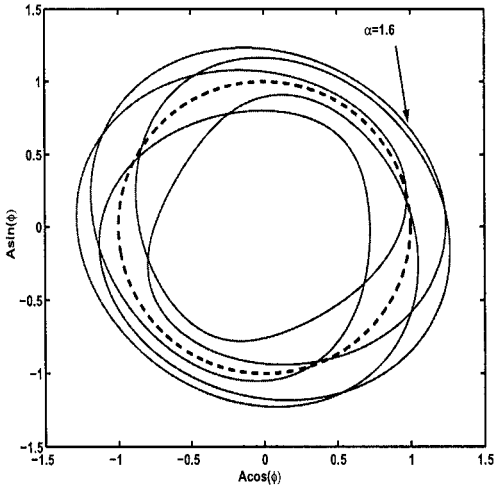

Figure 11. The periodic orbit of APM associated with the input $u(t) = u_1(t) + \sin(1{\cdot}6\omega_o t)$

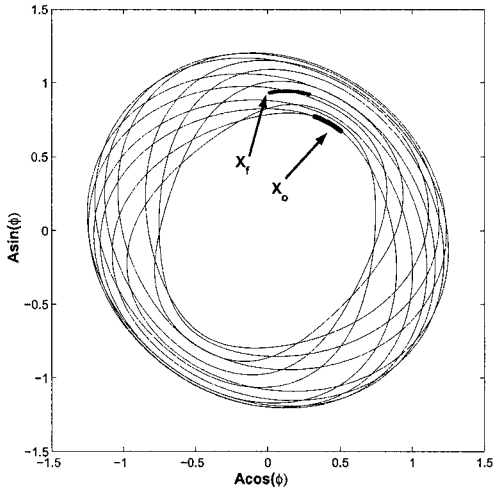

Figure 12. The phase portrait of APM associated with the input $u(t) = u_1(t) + \sin(\sqrt{3}\omega_o t)$

9. Conclusion

Mathematical properties of two nonlinear adaptive filters proposed by the authors are studied in this paper. The filters are useful in disturbance/noise detection, signal quality enhancement and system control and protection. It is shown that each of the dynamics of the filters possesses a unique and stable periodic orbit. Uniqueness and stability of the periodic orbits are mathematically proven. Computer simulations are performed to numerically verify the existence and properties of the periodic orbits. Finally, experimental results of the digital implementation are presented.

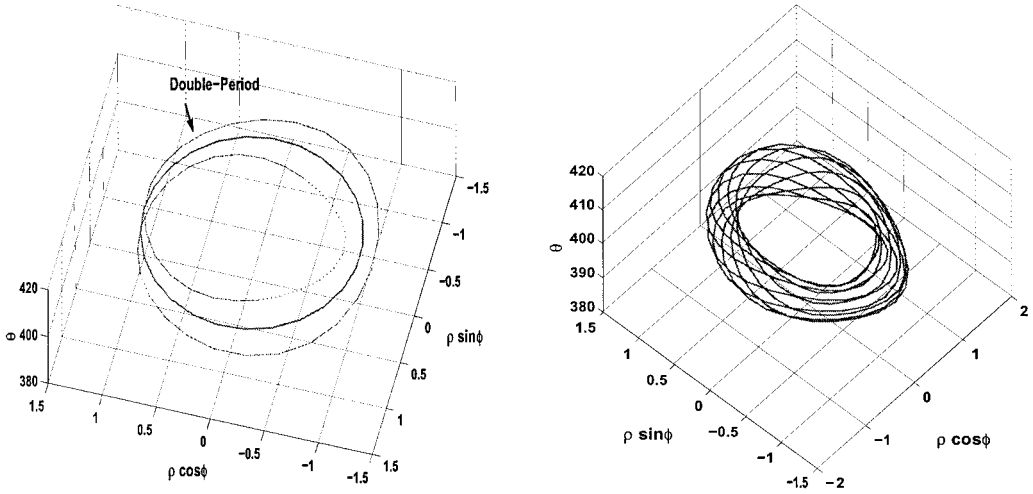

Figure 13. The phase portrait of APFM showing the phenomenon of generation of a double-period orbit and another orbit whose period is eight times the original one.

Appendix A. Averaging theorem

The averaging theorem which was used in the proof of Theorem 1 is reviewed here based on the expositions by Guckenheimer/Holmes [11, pp. 167–168] and Hale [12, Chapter V].

Consider the system

$$\dot{X} = \epsilon F(X, t, \epsilon); \qquad X \in U \subseteq \mathbb{R}^n, \quad 0 \leq \epsilon \ll 1, \tag{A1}$$

where $F : \mathbb{R}^n \times \mathbb{R} \times \mathbb{R}^+ \longrightarrow \mathbb{R}^n$ is C^r, $r \geq 2$, bounded on bounded sets, and of period $T > 0$ in t.

The associated autonomous averaged system is defined as

$$\dot{X}_a = \epsilon \frac{1}{T} \int_0^T F(X_a, t, 0)\mathrm{d}t := \epsilon \bar{F}(X_a) \tag{A2}$$

where the new variable X_a is the 'averaged' value of X.

Theorem 3. (The Averaging Theorem) There exists a C^r change of coordinates $X = X_a + \epsilon W(X_a, t, \epsilon)$ under which $(A1)$ becomes

$$\dot{X}_a = \epsilon \bar{F}(X_a) + \epsilon^2 F_1(X_a, t, \epsilon)$$

where F_1 is of period T in t. Moreover,

- If $X(t)$ and $X_a(t)$ are solutions of $(A1)$ and $(A2)$ based at X_0 and X_{a0}, respectively at $t = 0$, and $|X_0 - X_{a0}| = \mathcal{O}(\epsilon)$, then $|X(t) - X_a(t)| = \mathcal{O}(\epsilon)$ on a time scale $t \sim 1/\epsilon$.
- If P_0 is a hyperbolic fixed point of $(A2)$ then there exists $\epsilon_o > 0$ such that for all $0 < \epsilon < \epsilon_o$, $(A1)$ possesses a unique hyperbolic periodic orbit[1]: $\gamma_\epsilon(t) = P_o + \mathcal{O}(\epsilon)$ of the same stability type as P_o.
- If $X^s(t) \in W^s(\gamma_\epsilon)$ is a solution of $(A1)$ lying in the stable manifold of the hyperbolic periodic orbit $\gamma_\epsilon(t) = P_o + \mathcal{O}(\epsilon)$, $X_a^s(t) \in W^s(P_o)$ is a solution of $(A2)$ lying in the stable manifold of the hyperbolic fixed point P_o and $|X^s(0) - X_a^s(0)| = \mathcal{O}(\epsilon)$, then $|X^s(t) - X_a^s(t)| = \mathcal{O}(\epsilon)$ for $t \in [0, \infty)$. Similar results apply to solutions lying in the unstable manifolds on the time interval $t \in (-\infty, 0]$.

In other words, the averaging theorem explains that the solutions of the averaged system converge to those of the original system and moreover it relates the periodic orbits of the original system to the fixed points of the averaged system which may be much easier to analyze.

[1] γ_ϵ may be a trivial periodic orbit, $\gamma_\epsilon(t) = P_o$.

Appendix B. Poincaré-map theorem

The Poincaré-map theorem is reviewed here mainly based on the exposition in [13, p. 64]. Consider the following ordinary differential equation

$$\frac{\mathrm{d}x}{\mathrm{d}t} = f(x), \qquad x \in \mathbb{R}^n, \tag{B1}$$

where $f : U \to \mathbb{R}^n$ is C^r on some open set $U \subset \mathbb{R}^n$. Let $\phi(t, \cdot)$ denote the flow generated by $(B1)$. Suppose that $(B1)$ has a periodic solution of period T which we denote by $\phi(t, x_o)$, where $x_o \in \mathbb{R}^n$ is any point through which this periodic solution passes. Let Σ be an $n-1$ dimensional surface transverse to the vector field at x_o; we refer to Σ as a cross-section to the vector field $(B1)$. If f is C^r, we can find an open set $V \subset \Sigma$ such that the trajectories starting in V return to Σ in a time close to T. The map that associates points in V with their points of first return to Σ is called *Poincaré map,* which we denote by P.

Theorem 4. Poincaré Map A fixed point of P corresponds to a periodic orbit of $(B1)$. The stability type of the fixed point of P is the same as that of the periodic orbit $(B1)$. A period k point of P (*i.e.*, a point $x \in V$ such that $P^k(x) = x$ provided $P^i(x) \in V,\ i = 1, \cdots, k$) corresponds to a periodic orbit of $(B1)$ that pierces Σ k times before closing.

The Poincaré map is also defined for a time-periodic differential equation [13, p. 69]. The idea is to define the variable $\theta = \omega t$ and extend the n-dimensional system to $n+1$ equations ($\dot{\theta} = \omega$). The same results of the autonomous case are still valid [13, p. 70].

Appendix C. Implicit-function theorem

What follows is an account of the theorem according to [12, p. 8].

Theorem 5. Implicit Function Theorem Suppose $F : \mathbb{R}^m \times \mathbb{R}^n \to \mathbb{R}^m$ has continuous first partial derivatives and $F(0, 0) = 0$. If the Jacobian matrix $\partial F(x, y)/\partial x$ is non-singular, then there exists neighborhoods $U,\ V$ of 0 in $\mathbb{R}^m,\ \mathbb{R}^n$, respectively, such that for each fixed $y \in V$ the equation $F(x, y) = 0$ has a unique solution x in U. Furthermore, this solution can be given as $x = g(y)$, where g has continuous first derivatives and $g(0) = 0$.

References

1. R.N. Bracewell, *The Fourier Transform and its Applications*. New York: McGraw-Hill (1986) 474pp.
2. K. Morita, *Applied Fourier Transform*. Burke: IOS Press (1995) 433pp.
3. E.O. Brigham, *The Fast Fourier Transform and its Applications*. Englewood Cliffs: Prentice Hall (1988) 448pp.
4. A.A. Girgis and F.M. Ham, A quantitative study of pitfalls in the FFT. *IEEE Transact. Aerosp. Electr. Syst.* 16 (1980) 434–439.
5. D.V. Coury and H.G.F. Brito, Digital filters applied to computer relaying. *Proc. Intern. Conf. Power Syst. Technol.* 2 (1998) 1062–1066.
6. M. Karimi-Ghartemani and M.R. Iravani, A nonlinear adaptive filter for on-line signal analysis in power systems: applications. *IEEE Trans. Power Delivery* 17 (2002) 617–622.
7. A.K. Ziarani, *Extraction of Nonstationary Sinusoids*. Ph.D. Dissertation. University of Toronto (2002) 145pp.
8. M. Karimi-Ghartemani and M.R. Iravani, An alternative structure for phase-locked loop (PLL) system. *submitted to the IEEE Trans. Circuits Syst. I: Fundam. Theory Applic.* Manuscript no. MNS-802.
9. L. Hsu, R. Ortega and G. Damm, A globally convergent frequency estimator, *IEEE Trans. Automatic Control* 44 (1999) 698–713.
10. A.A. Giordano, *Least Square Estimation with Applications to Digital Signal Processing*. New York: John Wiley & Sons (1985) 412pp.
11. J. Guckenheimer and P. Holmes, *Nonlinear Oscillations, Dynamical Systems, and Bifurcations of Vector Fields*. New York: Springer Verlag (1983) 453pp.
12. J.K. Hale, *Ordinary Differential Equations*. New York: John Wiley & Sons (1969) 332pp.
13. S. Wiggins, *Introduction to Applied Nonlinear Dynamical Systems and Chaos*. New York: Springer-Verlag (1983) 672pp.
14. S. Kerbs, *UHP40 user's manual*. University of Toronto (1995).